# Numerical study of soap-film flow by nonuniform alternating electric fields

M. Nasiri, R. Shirsavar, and S. Mollaei
*Department of Physics, Faculty of Science, University of Zanjan, Zanjan, Iran*

A. Ramos
*Departamento de Electrónica y Electromagnetismo, Facultad de Física, Universidad de Sevilla, Sevilla, Spain*
(Received 29 October 2016; published 27 February 2017)

Fluid flow of suspended liquid films induced by non-uniform alternating electric fields has been reported. The electric fields were generated by two rod-like electrodes perpendicular to the fluid surface. The observed fluid flow was explained qualitatively by considering a *charge induction mechanism*, where the electric field actuates on the charge induced on the film surface. In this paper we perform a numerical study of this fluid flow taking into account the charge induction mechanism. The numerical results are compared with experiments and good agreement is found. Finally, we propose the application of the device as a new kind of *two dimensional fluid pump*.

DOI: 10.1103/PhysRevE.95.022806

## I. INTRODUCTION

The electrical manipulation of particles and fluids at the micrometer scale is a vibrant interdisciplinary field of study with promising applications in micro-electromechanical industry, chemical analysis, and/or biotechnology. One of the main goals is the development of 'lap-on-chip' or 'factory-on-chip' devices with integrated pumps, reagent dispensers, mixers, separators, and detection units that would automatically return data or products [1–3]. In this respect, liquid film flows induced by electric fields have recently been recognized as a method for nanofluidic manipulation in soft nanofluidics, i.e., systems where the fluid is confined between soft deformable surfaces [4].

Soap films as two-dimensional complex fluids have been studied by Gharib *et al.* [5], Chomaz *et al.* [6], and Rutgers *et al.* [7]. In these studies, the dominant forces were the gravitational force and the surface-air interaction. The electrohydrodynamics of films made of complex structured fluids have been studied by Faetti *et al.* [8,9] and Morris *et al.* [10,11]. They have shown that passing an electric current through nematic and smectic freely suspended liquid crystal films produces vortices on the film. Amjadi *et al.* [12] have shown controllable rotating flow on suspended water films by using, simultaneously, a current passing through the freely suspended film and an external electric field perpendicular to and in the plane of the electric current. The controllable rotation of fluid films has also been reported for polar liquid films [13] and MBBA liquid crystal films [14]. Saghaei *et al.* [15] presented a related experiment of liquid bulk rotation with one free surface. Nasiri *et al.* [16] have proposed an explanation of the water film rotation based on the electrical forces actuating on the charges induced on the free surface of an ohmic liquid.

Recent experiments have shown controllable flows in soap films induced by non-uniform alternating electric fields [17]. The electric fields were generated by two parallel metal cylinders that were perpendicular to the suspended soap film. The experiments were explained by taking into account the charge induced on the surface of the film. Here we perform a numerical analysis of these experiments taking into account the charge induction mechanism. The paper is organized as follows. First we explain the experimental setup and detail the experimental results. Then, we describe the hydrodynamic and electrical equations that govern the problem assuming that the liquid is characterized by its electrical conductivity and dielectrical permittivity, i.e., we assume the ohmic, or leaky dielectric, model [18]. Subsequently, we simulate the motion of the liquid film using the commercial finite element solver COMSOL and compare the numerical results with the experiments.

## II. EXPERIMENTS

### A. Experimental setup

Recently we have reported soap film flow induced by non-uniform alternating electric fields [17]. The AC electric fields are generated by two parallel metal cylinders connected to an AC power supply. The cross-section radius $R$ of the cylindrical electrodes is $0.50 \pm 0.01$ mm. The distance $\ell$ between the electrodes is fixed at $1.0 \pm 0.1$ cm. The applied ac voltage has an amplitude $V_0$ in the range 0–3 kV and a frequency in the range of 0–80 kHz. We investigated two possible setups: (1) The "disconnected" setup, in which both metal rods are perpendicular to the horizontally extended soap film and at a distance $h = 0.5 \pm 0.1$ mm from the film surface (Fig. 2(a)). (2) The "singly connected" setup, in which both metal rods are perpendicular to the horizontally extended soap film and one of the electrodes is connected to the film while the other remains disconnected (Fig. 1(a)). In these setups, the applied electric voltage passes an AC electrical current through the film since the disconnected electrodes are capacitively coupled to the liquid film.

By applying an AC electric voltage in the singly connected setup, a jet flow on the soap film can be observed. The direction of the jet flow is from the connected electrode towards the disconnected electrode. This jet flow produces two vortices rotating in opposite direction. Figures 1(b) and 1(c) show, respectively, the top view and particle image velocimetry (PIV) of a typical soap film in the singly connected setup. In the disconnected setup, there appear two jet flows on the film

 

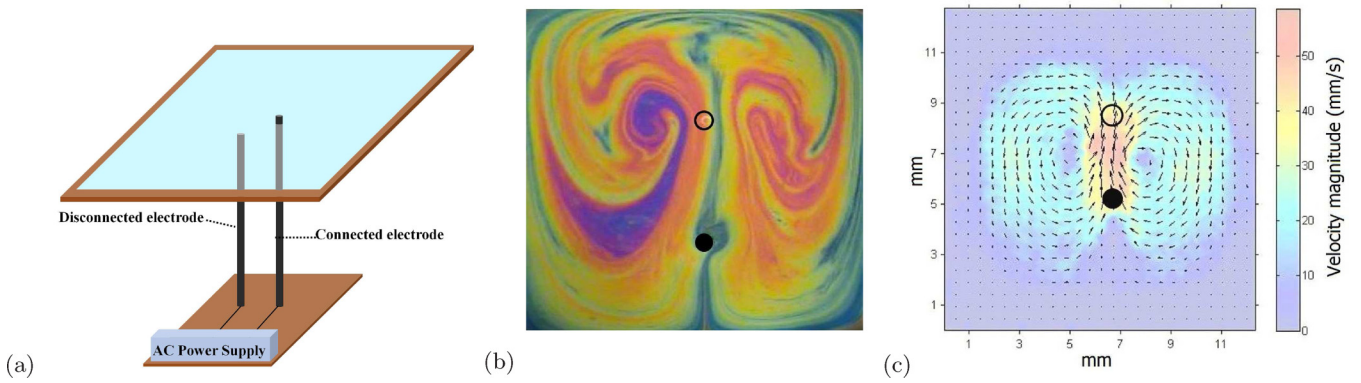


FIG. 1. The singly connected setup. (a) Setup for the experiment; (b) soap film top view; (c) PIV of soap film flow. The applied AC voltage had an amplitude of 3 kV and a frequency of 40 kHz.

from the midpoint between electrodes towards the electrodes. These two jet flows produce four vortices. Figures 2(b) and 2(c) show, respectively, the top view and PIV of a typical soap film in the disconnected setup. In both setups, flow velocity increases by increasing the amplitude of the applied signal, but the flow direction on soap films does not change with electric voltage amplitude [17].

### B. Experimental results

For the disconnected or the singly connected setup, under AC electric fields with frequencies lower than 1 kHz, fluid flow was negligible. Above 10 kHz, flow can easily be observed and measured. In the experiments, we increased the frequency up to 80 kHz. By increasing the frequency of the applied signal, the flow velocity increases although the flow pattern does not change. The measured values for the average velocity of jet flow versus frequency in the singly connected setup are shown in Fig. 3. Here the jet velocity was averaged in a small region close to the disconnected electrode. A quadratic polynomial fit is in excellent agreement with the experimental data, i.e., the average velocity of jet flow $\overline{v}_{\text{jet}}$ as a function of signal frequency $f$ follows $\overline{v}_{\text{jet}} \propto f^2$ in this limited range of frequencies. The observations imply that, at a constant applied voltage, increasing the frequency will rapidly increase the velocity of the jet flow [17].

## III. THEORY AND NUMERICAL SIMULATION

In this section we employ classical electrohydrodynamics to numerically study both setups. The equations will be solved using the commercial finite element solver COMSOL Multiphysics. Figure 4 shows the simulation domain for the disconnected setup (a) and for the connected setup (b). The domain consists of a two-dimensional (2D) fluid film surrounded by an air box. The rod-like electrodes are parallel cylinders with radius $R = 0.5$ mm and separated by a distance of $\ell = 1$ cm. The gap between electrodes and soap film is $h = 0.5$ mm for the disconnected case. For the connected case, one of the electrodes crosses the soap film and the other electrode is separated from the film by a gap of $h = 1$ mm. The air cube size is $4 \times 4 \times 4$ cm. The $2 \times 2$ cm liquid film is placed at the center of the geometry. The thickness of the actual soap film is very small ($d \sim 10$ nm–1 $\mu$m) in the experiments. Therefore, and in order to avoid mesh-size limitations in the finite element simulations, the film can be considered to be a two-dimensional surface with appropriate electrical and mechanical 2D properties (see below).

We will consider the liquid to be characterized by its electrical conductivity $\sigma_{\text{film}}$ and dielectric permittivity $\varepsilon_{\text{film}} = 7.08 \times 10^{-10}$ F/m (water permittivity). As mentioned before, the Coulomb force acting on the induced surface charge is responsible for the fluid motion. Therefore, we use the ohmic—or leaky dielectric—model to explain the

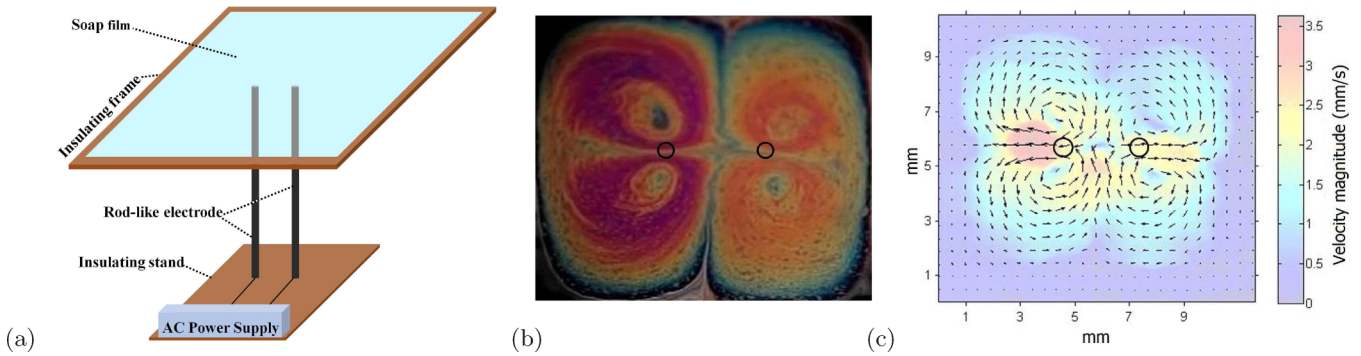


FIG. 2. The disconnected setup. (a) Setup for the experiment; (b) soap film top view; (c) PIV of soap film flow. The applied AC voltage had an amplitude of 3 kV and a frequency of 20 kHz.

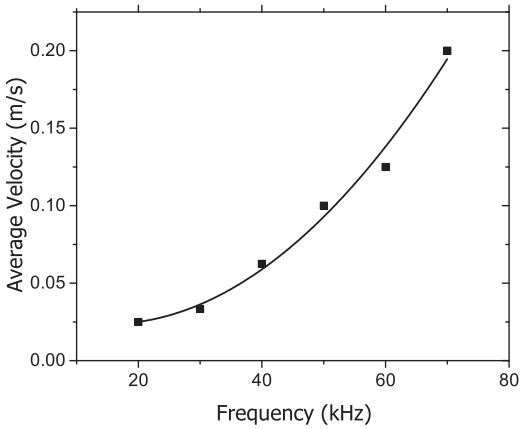


FIG. 3. Average jet flow velocity versus frequency of applied electric voltage for the singly connected setup. The applied voltage amplitude is 3 kV. The soap film surface is approximately 4 $cm^2$, the distance between electrodes $\ell = 1$ cm, the gap between disconnected electrode and film $h = 1$ mm and the radius of cylindrical electrodes $R = 0.5$ mm.

electrohydrodynamics of the fluid. In this model, induced charges appear at interfaces when dealing with homogeneous liquids [19]. These induced charges are considered to be superficial, although in reality they extend from the film surface up to some typical distance of the order of the Debye length, $\lambda_D$. Therefore, the model considers that the Debye length is much smaller than the thickness of the film, $\lambda_D \ll d$. In the experiments of Ref. [17], the concentration of $H^+$ due to the addition of ionic surfactant to the soap film leads to an estimated Debye length of the order of several nanometers.

For the sake of simplicity, surface tension contribution to fluid motion is neglected in this work. Surface tension provides the mechanical stability of the water film along the surface normal direction.

The equations that we use in order to describe the fluid motion are the following:

### A. Electrical equations

Inside the simulation box the time-harmonic fields are governed by the continuity of the total electrical current (ohmic plus displacement currents) that in phasor notation reads

$$\nabla \cdot (\sigma \mathbf{E} + i\omega\varepsilon \mathbf{E}) = 0, \tag{1}$$

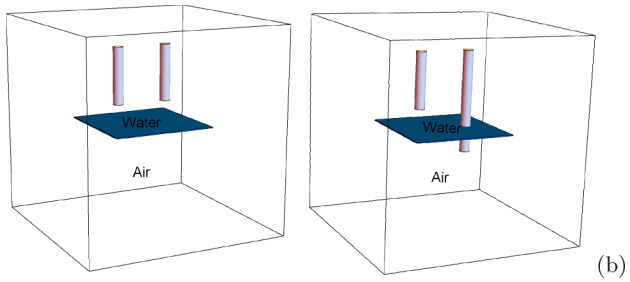


(a) (b)

FIG. 4. Simulation setup: (a) Case of disconnected electrodes; (b) Case of singly connected electrode.

where the electric field is irrotational $\mathbf{E} = -\nabla\phi$, $\phi$ is the electric potential phasor, and $\omega = 2\pi f$ is the angular frequency. In our case the medium is air with zero conductivity and $\varepsilon = 8.85 \times 10^{-12}$ F/m. The 2D film is taken into account in the electrical problem as a boundary condition:

$$\mathbf{n} \cdot (\mathbf{J}_2 - \mathbf{J}_1) = -\nabla_s \cdot (d(\sigma_{\text{film}} + i\omega\varepsilon_{\text{film}})\nabla_s\phi), \tag{2}$$

where $\mathbf{J}_2$ and $\mathbf{J}_1$ are current densities on both sides of the film and $\mathbf{n}$ is the normal vector of the surface pointing from 1 to 2. This boundary condition comes from the continuity of the total current: the current jump across the surface is equal to the surface divergence of current [20]. Notice that current densities include the displacement current, i.e., $\mathbf{J} = \sigma\mathbf{E} + i\omega\varepsilon\mathbf{E}$, which becomes $\mathbf{J} = i\omega\varepsilon\mathbf{E}$ for air. The operator $\nabla_s$ is 2D nabla operator acting tangentially to the surface. In Eq. (2), the film electrical conductivity $\sigma_{\text{film}}$ and permittivity $\varepsilon_{\text{film}}$ are multiplied by the film thickness $d$, which implies that 2D films are fully characterized by the following electrical 2D properties: $\bar{\sigma} = d\sigma_{\text{film}}$ and $\bar{\varepsilon} = d\varepsilon_{\text{film}}$. The remaining boundary conditions are those of fixed potential at the cylindrical electrodes and normal total current equal to zero at outer surfaces.

Once the electric field has been obtained, the electrical stress actuating upon the liquid film can be computed. The surface charge density times the tangential electric field provides the Coulomb force that will be used as body force in the 2D hydrodynamic equations actuating on the fluid film [16]. The surface charge density on the 2D film is given by the discontinuity of the normal component of the electric displacement field:

$$q_s = \varepsilon(\mathbf{E}_2 - \mathbf{E}_1) \cdot \mathbf{n}, \tag{3}$$

where $\mathbf{E}_2$ and $\mathbf{E}_1$ are the electric fields at both sides of the film surface and $\mathbf{n}$ is the normal to the surface pointing from 1 to 2. The surface charge expression (3) should be corrected if the electric flux flowing inside the film gets to be important. In this case, the free charge per unit area becomes: $q_s = \varepsilon(\mathbf{E}_2 - \mathbf{E}_1) \cdot \mathbf{n} + d\varepsilon_{\text{film}}\nabla_s \cdot \mathbf{E}_s$. This expression should be used at high frequencies ($\omega\varepsilon_{\text{film}} \gg \sigma_{\text{film}}$) where induced free charge on the film goes to zero.

### B. Hydrodynamic equations

As the film thickness is very small, we characterize the water film as a two-dimensional fluid medium with material parameters, $\bar{\rho} = \rho d$, $\bar{\eta} = \eta d$, where $\rho$ is the fluid bulk mass density and $\eta$ is the dynamic viscosity. The 2D fluid velocity $\mathbf{u} = (u, v)$ is governed by the 2D Navier-Stokes equations, that in steady state are

$$\bar{\rho}(\mathbf{u} \cdot \nabla_s)\mathbf{u} = -\nabla_s \bar{p} + \bar{\eta}\nabla_s^2\mathbf{u} + \mathbf{F}_e, \tag{4}$$

$$\nabla_s \cdot \mathbf{u} = 0, \tag{5}$$

where $\bar{p} = pd$ is the 2D pressure field and $\mathbf{F}_e$ is the time-averaged tangential electrical stress acting on the 2D fluid. The fluid parameters are $\rho = 1100\,\text{kg/m}^3$ and $\eta = 0.003$ Pa s [16]. In the low Reynolds regime, Re $\ll 1$, which is fulfilled in our problem, it is possible to use Stokes equation to describe the fluid flow. The AC signals employed in the experiments have periods much shorter than the typical mechanical time scales of the fluid, then the electrical stress, $\mathbf{F}_e$, is given by the

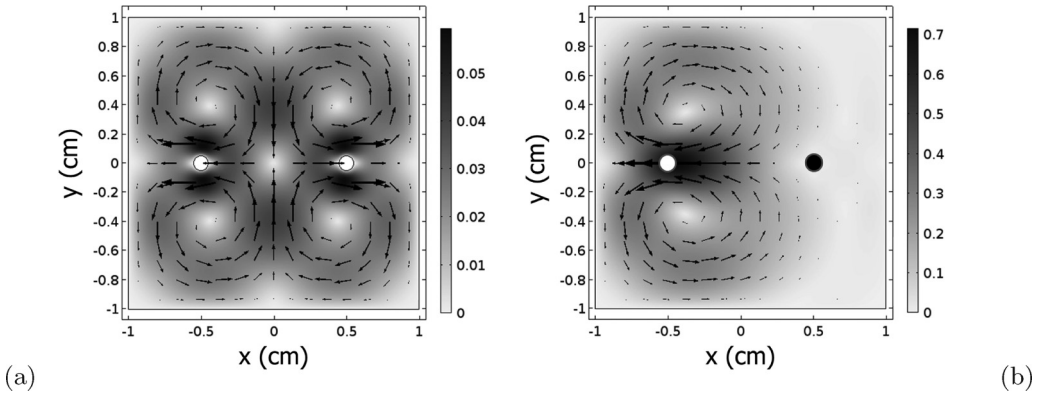


FIG. 5. Two-dimensional fluid flow for $V_0 = 3\,\text{kV}$ and $f = 40$ kHz. The empty (filled) circles show the disconnected (connected) electrodes: (a) Disconnected electrodes case, and (b) singly connected case. Velocity amplitude is given in m/s.

time-averaged Coulomb force per unit area acting on the film $\mathbf{F}_e = \langle q_s(t)\mathbf{E}_s(t)\rangle$, which can be written using phasors as

$$\mathbf{F}_e = \tfrac{1}{2}\text{Re}(q_s\mathbf{E}_s^*). \tag{6}$$

This last equality holds for the time-averaged product of two oscillating functions of the same frequency. Here, Re$(\cdots)$ stands for "the real part of..." and $\mathbf{E}_s^*$ is the complex conjugate of the tangential electric field phasor.

The boundary conditions for the hydrodynamic equations are those of no-slip $\mathbf{u} = 0$ on the frame walls, and on the electrode-film boundary for the case of singly connected electrode.

## IV. RESULTS

In this section we choose some experimentally accessible parameters to simulate both setups shown in Fig. 4. Figure 5 shows the velocity field vector $(u,v)$ for disconnected and singly connected configurations. A comparison of the simulation results with experimental fluid flow patterns (Figs. 2(b) and 1(b)) is in good agreement. In the disconnected case, there are four vortices (two rotating clockwise and two anticlockwise) placed symmetrically within the square frame. In the singly connected case there is a jet-like flow from connected to disconnected electrode, which produces two vortices which rotate in opposite directions. The amplitude of the velocity obtained numerically is greater than in the experiments. Here we have employed a viscosity value of 0.003 Pa s for our water glycerol solution. However, it is supposed to be much greater for soap films due to the effect of surface viscosity [16], and the increased viscous stresses would significantly reduce the experimental velocity. In the simulations and in the experiments, the singly connected case generates greater velocities than the disconnected case for the same applied signal. As a possible explanation, we observe that the electrical force is directed mainly in one direction in the singly connected case (towards the disconnected electrode), while in the disconnected case the electrical force is mainly directed in opposite directions (towards the two electrodes).

Figure 6 shows the absolute value of flow velocity along $x = -0.4$ cm for the singly connected case (see Fig. 5(b)). There is a maximum around $y = 0$ which reveals that there is a narrow region (jet flow) near the line joining the electrodes where the fluid velocity is higher. The point $(x = -0.4, y = 0)$ is the point where flow velocity was measured in experiments and it is close to the point of maximum velocity.

Figure 7 depicts the average velocity of the jet flow versus the ratio between signal frequency and film conductivity in a log-log plot for different values of film conductivity. As can be seen, the plots for the different conductivities are coincident, demonstrating that the velocity depends on the parameter combination $f/\sigma$ in our model. Here the average velocity of the jet flow was measured as in experiments under the disconnected electrode (point $x = -0.4, y = 0$). It was defined as $\bar{v}_{\text{jet}} = \frac{1}{L}\int_{-L/2}^{L/2}|\mathbf{u}|dy$, where $L = 2\,\text{mm}$ along $y$ direction as the width of jet flow. The figure shows that fluid velocity depends on the parameter $f/\sigma$. For low values of $f/\sigma$, it can be seen that $v_{\text{jet}} \propto (f/\sigma)^2$, in agreement with the experimental observations of Fig. 3. Figure 7 shows a maximum velocity around $f/\sigma = 1$ MHz/(S/m). This frequency is closely related to the characteristic frequency of the RC circuit formed by the capacitance between the disconnected electrode and the liquid film $C$, and the resistance of the liquid film $R$.

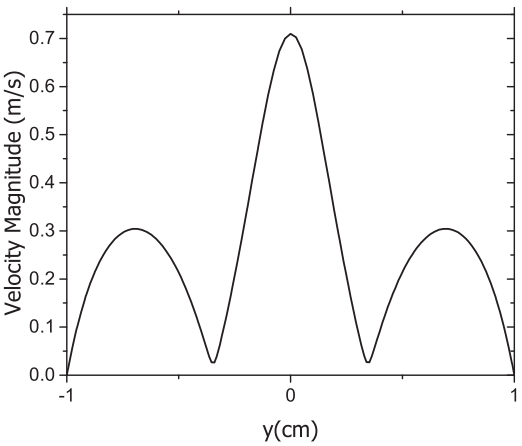


FIG. 6. Velocity magnitude profile for the singly connected setup along $x = -0.4$ cm for an applied signal of $V_0 = 3\,\text{kV}$ and $f = 200$ kHz. There is a jet flow from the connected electrode to the disconnected one. The parameters of the film are $\eta = 0.003$ Pa s, $d = 1\,\mu\text{m}$, $\sigma = 0.8$ S/m.

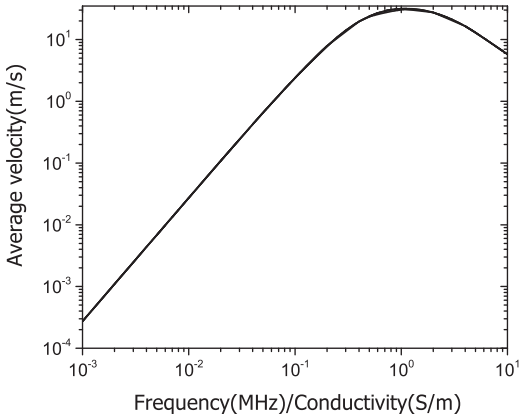


FIG. 7. Average jet velocity vs (frequency/conductivity) for different values of the film conductivity $\sigma = 0.05, 0.1, 0.2, 0.4, 0.8$ S/m. The figure shows that fluid velocity depends on the parameter combination (frequency/conductivity).

This RC characteristic frequency can be seen in the simulations shown in Fig. 8(a). The figure shows real and imaginary parts of the electrical current between electrodes as a function of frequency, as computed using finite elements, for a voltage amplitude of 1 kV. The plot depicts current intensity divided by film conductivity versus signal frequency divided by film conductivity. The current flows between electrodes mainly following the two branches of an equivalent circuit [see Fig. 8(b)]. The first branch consists of the capacitance between the two electrodes through air ($C_{\text{air}}$). The second branch is the previously mentioned RC circuit which is the series combination of the capacitance between disconnected electrode and film, $C$, plus the film resistance, $R$. Using this equivalent circuit, real and imaginary parts of the electrical current are given by

$$I_{\text{Re}} = \frac{(\omega C)^2 R}{1 + (\omega C R)^2} V, \tag{7}$$

$$I_{\text{Im}} = \frac{(\omega C)}{1 + (\omega C R)^2} V + \omega C_{\text{air}} V. \tag{8}$$

The computed values of Fig. 8 follow these expressions as a first approximation. The imaginary current is mainly given by the displacement current through air between electrodes (dashed line in the figure). The real current is mainly given by the ohmic current through the film (solid line in the figure). From the comparison with the expressions, the characteristic RC frequency can be obtained as $f_{RC} = 1/(2\pi RC) \approx 0.7 \times \sigma_{\text{film}}$ MHz/(S/m).

We now analyze the voltage and current for the RC branch [see solid line of Fig. 8(a)]. At very low frequencies, there is negligible current and most of the voltage is dropped across the gap between electrode and film (with capacitance $C$). For these frequencies, the soap film is almost equipotential. In this situation there is induced charge on the film but negligible tangential electric field and force. At high frequencies, current intensity reaches maximum values, the impedance of the capacitor is much smaller than the film resistance $R$, and the voltage is mainly dropped across the film resistance. In this situation there is tangential electric field on the film but negligible surface charge and, therefore, negligible force. For intermediate frequencies there are both induced charge and tangential electric field, so that there is Coulomb force acting on the fluid film. This intermediate frequency corresponds to the frequency of maximum velocity in Fig. 7, and it is closely related to the RC frequency of Fig. 8.

A quantitative comparison is more difficult given the uncertainty of some magnitudes, namely, effective viscosity, film conductivity, and film thickness. In Ref. [16], liquid film was assumed to have an effective viscosity around 40 times the bulk viscosity of the water/glycerol mixture (0.003 Pa s) in order to match theory and experiments. The reason for this increment in viscosity is the existence of an extra 2D surface viscosity due to the surfactant-laden interfaces (top and bottom). According to Ref. [21], surface viscosity is very sensitive on the surfactant concentration and can easily be between 0.02 and 0.1 $\mu$Pa s m. If we assume that the film effective viscosity is 40 times greater than the bulk viscosity, the theoretical velocity would be around 40 times smaller. Therefore, a velocity of 0.2 m/s in Fig. 3 (with $f = 70$ kHz)

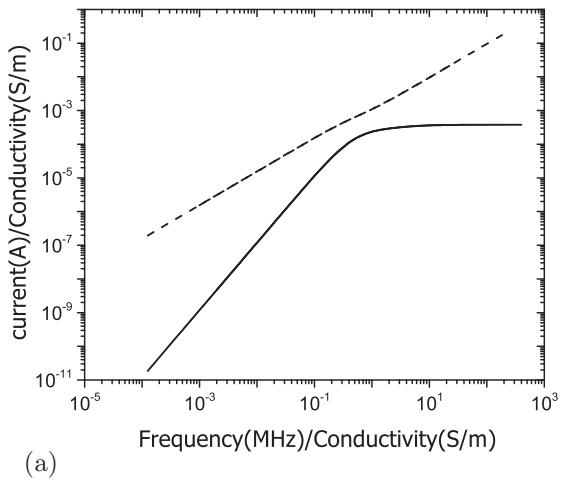


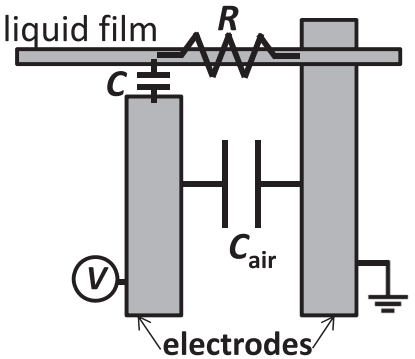


FIG. 8. (a) Current intensity between electrodes as a function of frequency. The plot shows real and imaginary parts of (intensity/conductivity) versus (frequency/conductivity) for a voltage amplitude of 1 kV. The dashed line corresponds to the imaginary part and the continuous line to the real part. (b) Equivalent electrical circuit of the system.

would correspond to a theoretical velocity around 8 m/s in Fig. 7 [with $f/\sigma = 0.2$ MHz/(S/m)]. This implies that the expected conductivity of the film is $\sigma_{\text{film}} = 0.35$ S/m. This value is of the order of the film conductivity that was assumed in [16] of $\sigma_{\text{film}} = 0.05$ S/m. To improve the comparison, the experimental values of the 2D viscosity and 2D conductivity of the film should be measured.

## V. CONCLUSIONS

The fluid flow of suspended liquid films induced by non-uniform alternating electric fields was reported by Shirsavar *et al.* [17]. The observed fluid flow was explained qualitatively by considering a *charge induction mechanism*, where the electric field actuates on the free charge induced on the film surface. In the present work we have performed a numerical study of the fluid flow taking into account the charge induction mechanism. Electrical and hydrodynamic equations were solved by using finite elements. In the simulations, the liquid film was considered a two-dimensional surface, both for the electrical and hydrodynamic problems. The numerical results were compared with experiments and good semi-quantitative agreement was found. To improve the quantitative comparison, new experiments would be required where the 2D viscosity and 2D conductivity of the film were measured.

Given the difficulty of measuring soap film viscosities, this kind of experiments could be useful to measure it, provided we can measure the electrical parameters of the system. For example, the resistance of the film could be measured during the film flow experiments by measuring the system impedance.

The singly connected device produces a jet flow in the interior region, which pumps fluid from the connected to the disconnected electrode. This means that we can propose a two-dimensional fluid pump.

## ACKNOWLEDGMENTS

A.R. acknowledges financial support from the Spanish Ministry Ministerio de Economía y Competitividad under Contract No. FIS2014-54539-P.

[1] A. Manz, N. Graber, and H. M. Widmer, Sensors and Actuators B (Chemical) **1**, 244 (1990).
[2] H. A. Stone, A. D. Stroock, and A. Ajdari, Annu. Rev. Fluid Mech. **36**, 381 (2004).
[3] M. P. Hughes, Nanotechnology **11**, 124 (2000).
[4] O. Bonhomme, O. Liot, A.-L. Biance, and L. Bocquet, Phys. Rev. Lett. **110**, 054502 (2013).
[5] M. Gharib and P. Derango, Physica D: Nonlinear Phenomena **37**, 406 (1989).
[6] J. M. Chomaz and B. Cathalau, Phys. Rev. A **41**, 2243(R) (1990).
[7] M. Rutgers, R. Bhagavatula, A. Petersen, W. Goldburg *et al.*, Phys. Fluids **8**, 2847 (1996).
[8] S. Faetti, L. Fronzoni, and P. Rolla, J. Chem. Phys. **79**, 5054 (1983).
[9] S. Faetti, L. Fronzoni, and P. Rolla, J. Chem. Phys. **79**, 1427 (1983).
[10] S. W. Morris, J. R. de Bruyn, and A. D. May, Phys. Rev. Lett. **65**, 2378 (1990).
[11] Z. A. Daya, S. W. Morris, and J. R. de Bruyn, Phys. Rev. E **55**, 2682 (1997).
[12] A. Amjadi, R. Shirsavar, N. H. Radja, and M. Ejtehadi, Microfluidics and nanofluidics **6**, 711 (2009).
[13] R. Shirsavar, A. Amjadi, A. Tonddast-Navaei, and M. Ejtehadi, Exp. Fluids **50**, 419 (2011).
[14] R. Shirsavar, A. Amjadi, M. Ejtehadi, M. Mozaffari, and M. Feiz, Microfluidics and Nanofluidics **13**, 83 (2012).
[15] T. Saghaei, A.-R. Moradi, R. Shirsavar, and M. Habibi, Appl. Phys. Lett. **106**, 053506 (2015).
[16] M. Nasiri, R. Shirsavar, T. Saghaei, and A. Ramos, Microfluidics and Nanofluidics **19**, 133 (2015).
[17] R. Shirsavar, A. Ramos, A. Amjadi, J. Taherinia, M. Mashhadi, and A. Nejati, J. Electrost. **73**, 112 (2015).
[18] D. Saville, Annu. Rev. Fluid Mech. **29**, 27 (1997).
[19] J. Melcher and G. Taylor, Annu. Rev. Fluid Mech. **1**, 111 (1969).
[20] L. Krahenbuhl and D. Muller, IEEE Trans. Magn. **29**, 1450 (1993).
[21] P. Stevenson, J. Colloid Interface Sci. **290**, 603 (2005).